Mathematical Biosciences and Engineering

http://www.aimspress.com/journal/mbe

MBE, 20(9): 17272–17295.
DOI: 10.3934/mbe.2023769
Received: 06 May 2023
Revised: 24 July 2023
Accepted: 08 August 2023
Published: 5 September 2023

Research article

QSPR/QSAR analysis of some eccentricity based topological descriptors of antiviral drugs used in COVID-19 treatment via $\mathcal{D}\varepsilon$- polynomials

Deepalakshmi Sarkarai and Kalyani Desikan*

Division of Mathematics, School of Advanced Sciences, Vellore Institute of Technology, Chennai, India

* **Correspondence:** Email: kalyanidesikan@vit.ac.in.

Abstract: In the field of chemical and medical sciences, topological indices are used to study the chemical, biological, clinical, and therapeutic aspects of pharmaceuticals. The COVID-19 pandemic is largely recognized as the most life-threatening crisis confronting medical advances. Scientists have tested various antiviral drugs and discovered that they help people recover from viral infections like COVID-19. Antiviral medications, such as Arbidol, Chloroquine, Hydroxy-Chloroquine, Lopinavir, Remdesivir, Ritonavir, Thalidomide and Theaflavin, are often used to treat COVID-19. In this paper, we define Diameter Eccentricity Based vertex degree and employ it to introduce a new polynomial called $D\varepsilon-$ Polynomial. Using the newly introduced polynomial, we derive new topological indices, namely, diameter eccentricity based and hyper diameter eccentricity based indices. In order to check the efficacy of our indices, we derive the $D\varepsilon-$ polynomials for the eight COVID-19 drugs mentioned above. Using these polynomials, we compute our proposed topological descriptors for the eight COVID-19 drugs. We perform quantitative structure-property relationship (QSPR) analysis by identifying the best fit curvilinear/multilinear regression models based on our topological descriptors for 8 physico- chemical properties of the COVID-19 drugs. We also perform quantitative structure-activity relationship (QSAR) analysis by identifying the best fit multilinear regression model for predicting the IC_{50} values for the eight COVID-19 drugs. Our findings and models may be useful in the development of new COVID-19 medication.

Keywords: diameter; eccentricity; molecular descriptors; QSPR/QSAR; anti-viral drugs

1. Introduction

A topological index is a mathematical measure that can be computed from chemical structures and can be depicted as simple graphs. They play an important role in the study of QSPR and QSAR. In theoretical chemistry, molecular structure descriptors (also called topological indices) are used for

modeling physico-chemical, pharmacological, toxicological, biological and other properties of chemical compounds. Chemoinformatics is an active area of research where quantitative pattern behavior and structure-property relations detect biological processes and other properties [1].

The chemical graph theory is a branch of graph theory that is concerned with analyses of all consequences of connectivity in a chemical graph. A structural formula of a chemical compound can be represented by a molecular graph which is used to characterize a molecule by depicting the atoms as the vertices of the graph and the molecular bonds as the edges. In chemistry, molecular topological indices, also known as topological indices, are utilized. Wiener [2] was the first to demonstrate that the Wiener index is strongly connected to the boiling points of alkanes. Feng et al. [3] provided a necessary criterion for a graph to be 'l-connected' in 2017 using the well-known Wiener index and Harary index. Su et al. [4] discussed the sufficient condition used with the forgotten topological index.

To predict physico-chemical properties and bioactivity of chemical compounds in QSPR/QSAR investigation, topological indices are employed. Zagreb indices [5, 6] are among the most effective for identifying physical attributes and chemical processes of chemical compounds. Gutman and Trinajstic [7] considered the first Zagreb index $M_1(G)$ and the second Zagreb index $M_2(G)$ for the first time in 1972. Ghobadi and Ghorbaninejad [8] developed accurate formulae for the Zagreb and Hyper-Zagreb indices of some molecular graphs in 2018. They defined the Forgotten topological index or super F-index, a novel distance-based Zagreb index. Estrada et al. [9] developed the Atom-Bond Connectivity (ABC) index, while Vukicevic and Furtula [10] introduced the geometric-arithmetic index. Gutman [11] proposed a novel graph-based topological index, the Sombor index. The index was initially used in chemistry, but it quickly piqued the curiosity of mathematicians [12]. Randic index is one of the oldest, most often used and most successful topological indices in QSPR and QSAR. Bollabas and Erdos [13] later proposed the generalized Randic index. The Harmonic index is a version of the Randic index, which was initially presented by Fajtlowicz [14].

The physico-chemical properties and biological activities of a compound are crucial in the development of pharmaceutical drugs. Many researchers are working on the QSPR analysis of various chemical compounds [15, 16], since it is an economically efficient approach to test a compound instead of testing the compounds in a wet lab. Gupta, Singh and Madan [17] proposed a unique graph invariant for predicting biological and physical features using the eccentric distance sum index (EDS). This topological index has a wide range of possible applications in the structure activity/property interactions of molecules, and it has a high discriminating power for both biological activities and physical characteristics. Hua, Xu and Shu [18] obtained a strong lower bound on the EDS index of n-vertex cacti. Yu, Feng and Ili'c [19] investigated the lower and upper bounds of the EDS index in terms of other graph invariants such as the Wiener index, the degree distance index, the eccentric connectivity index and so on.

Chemical qualities, physical properties, pharmacological properties and biological properties of medications are all important in medical research for drug creation. Topological indices can be used to identify these features [20]. Recently, researchers have started researching topological indices and COVID-19 medications. In addition, the following studies are notable in the investigation of medications repurposed against SARS-CoV-2 [21]. Kirmani et al. [22] established QSPR models with linear regression between physico-chemical properties of potential antiviral drugs and some topological indices for various antiviral drugs used in the treatment of COVID-19 patients. Shirkol et al. [23] investigated the predictive power of degree-distance and distance-based topological indices through

QSPR analysis. Similarly, Lučić et al. [24] performed QSPR analysis using novel distance-related indices.

Deutsch and Klavžar [25] defined the M-Polynomial in 2015. Using the edge partition technique, $M-$ Polynomial is employed to perform degree based computations. It is crucial in calculating the exact expressions of several degree-based topological indices. The Neighborhood $M-$ polynomial ($NM-$ Polynomial) was introduced by Mondal et al. [26]. It performs the same functions as the $M-$ polynomial for neighborhood degree sum-based indices. It is used to make computations related to neighborhood degree sum-based indices easier. These polynomials are determined by the sum of neighboring vertex degrees. The $RNM-$ polynomial is used to evaluate several forms of reduced neighborhood indices [27].

In this paper, we have considered some antiviral drugs that are used for the treatment of COVID−19 patients, namely, Arbidol, Chloroquine, Hydroxy-Chloroquine, Lopinavir, Remdesivir, Ritonavir, Thalidomide and Theaflavin. We have introduced a new type of vertex degree called Diameter Eccentricity Based vertex degree and employed it to introduce a new polynomial called $\mathcal{D}\varepsilon$-polynomial. We use the newly introduced polynomial to derive our proposed topological indices. We further check the applicability of our indices by deriving the $\mathcal{D}\varepsilon$-polynomials for the eight afore-mentioned COVID-19 drugs. We perform Quantitative Structure-Property Relationship (QSPR) analysis by arriving at the best fit curvilinear and multilinear regression models based on our topological descriptors for 8 physico-chemical properties of the COVID-19 drugs. We also perform Quantitative Structure-Activity Relationship (QSAR) analysis and identify the best fit multilinear regression model to predict the IC_{50} values of the eight COVID-19 drugs.

Let G be a simple, finite and connected graph with vertex set as $V(G)$ and edge set as $E(G)$. Let d_p denote the degree of a vertex p in G and ε_p the eccentricity of the vertex p. Let $\Delta(G)$ denote the maximum degree and $\delta(G)$ denote minimum degree among the vertices of G, respectively.

Definition 1.1. *[28] The eccentricity index for a graph G is defined as*

$$\varepsilon(G) = \sum_{pq \in E} \left[\varepsilon_p + \varepsilon_q\right] \tag{1.1}$$

where ε_p denotes the eccentricity of the vertex p.

Definition 1.2. *[29] The Ediz eccentric connectivity index $E\mathcal{E}^c(G)$ of G is defined as*

$$E\mathcal{E}^c(G) = \sum_{v \in V(G)} \frac{S(v)}{\varepsilon(v)} \tag{1.2}$$

where $S(v)$ is the sum of degrees of all vertices adjacent to vertex v and $\varepsilon(v)$ is the eccentricity of the vertex v.

The Revan vertex degree of p in G is defined as $r_p = \Delta(G) + \delta(G) - d_p$. Based on the Revan vertex degree, Revan indices were introduced by Kulli [30, 31]. He has studied oxide networks, honeycomb networks, drugs and antibiotic structures with the help of Revan and Banhatti indices [32]. Inspired by this definition, we have introduced and defined a new type of vertex degree called Diameter Eccentricity Based vertex degree of p in G as

$$d\varepsilon_p = D(G) + 1 - \varepsilon_p$$

where $D(G)$ denotes the diameter of the graph G.

Figure 1 shows the eccentricity and diameter eccentricity based vertex degrees ($d\varepsilon-$values) of the Tadpole Graph $T(3,2)$.

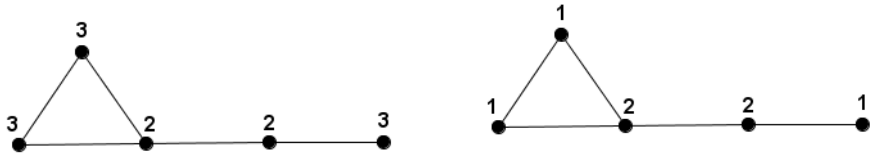

Figure 1. Eccentricity and $d\varepsilon-$values.

Eccentricity of a vertex is a measure of the centrality of a vertex. Diameter, on the other hand, is a global entity with respect to the graph, that can be considered as a measure of the spread of the graph. Our diameter eccentricity based vertex degree captures both these measures and determines the importance of a vertex with respect to the whole graph..

Based on this new vertex degree definition, we define diameter eccentricity based and hyper diameter eccentricity based indices for any connected graph G by introducing a new polynomial called $D\varepsilon-$polynomial as

$$\mathcal{D}\varepsilon(G) = \sum_{i\leq j} (\text{number of edges } pq \text{ such that } d\varepsilon_p = i, d\varepsilon_q = j)\alpha^i\beta^j = \sum_{i\leq j} r\rho_{(i,j)}\alpha^i\beta^j = f(\alpha,\beta) \quad (1.3)$$

where $r\rho_{(i,j)}$ denotes the number of edges in the edge partition and α,β are variables. Our $\mathcal{D}\varepsilon-$ Polynomial is a function of α and β. It is dependent on the diameter eccentricity based vertex degrees of the end vertices of the edges of the graph. The $M-$ polynomial, $NM-$ polynomial and $RNM-$ polynomial can be used to derive degree based, neighborhood degree based and reverse neighborhood degree based indices. Our polynomial is novel and the first of its kind related to eccentricity based indices.

In Table 1, we introduce our new indices as functions of $d\varepsilon_p$ and $d\varepsilon_q$

Table 1. Description of proposed indices.

Indices	$f(d\varepsilon_p, d\varepsilon_q)$
First $\mathcal{D}R\varepsilon$ Index ($\mathcal{D}R_1\varepsilon$)	$d\varepsilon_p + d\varepsilon_q$
Second $\mathcal{D}R\varepsilon$ Index ($\mathcal{D}R_2\varepsilon$)	$d\varepsilon_p * d\varepsilon_q$
First Hyper $\mathcal{D}R\varepsilon$ Index (H$\mathcal{D}R_1\varepsilon$)	$(d\varepsilon_p + d\varepsilon_q)^2$
Second Hyper $\mathcal{D}R\varepsilon$ Index (H$\mathcal{D}R_2\varepsilon$)	$(d\varepsilon_p * d\varepsilon_q)^2$

Our diameter eccentricity based indices, that is $\mathcal{D}R_1\varepsilon$ and $\mathcal{D}R_2\varepsilon$ and the Hyper Diameter Eccentricity Based indices, that is $H\mathcal{D}R_1\varepsilon$ and $H\mathcal{D}R_2\varepsilon$ indices can be derived using our $\mathcal{D}\varepsilon$-polynomial.

Table 2 shows the formulae for deriving our indices using the $\mathcal{D}\varepsilon$-polynomial

Table 2. Derivation of proposed indices from $\mathcal{D}\varepsilon$-polynomial.

Indices	Derivation from $\mathcal{D}\varepsilon(G)$
$\mathcal{D}R_1\varepsilon$	$\left(\partial_\alpha + \partial_\beta\right)\left(\mathcal{D}\varepsilon(G)\right)\Big\vert_{\alpha=1,\beta=1}$
$\mathcal{D}R_2\varepsilon$	$\left(\partial_\alpha * \partial_\beta\right)\left(\mathcal{D}\varepsilon(G)\right)\Big\vert_{\alpha=1,\beta=1}$
$\mathrm{H}\mathcal{D}R_1\varepsilon$	$\left(\partial_\alpha + \partial_\beta\right)^2\left(\mathcal{D}\varepsilon(G)\right)\Big\vert_{\alpha=1,\beta=1}$
$\mathrm{H}\mathcal{D}R_2\varepsilon$	$\left(\partial_\alpha * \partial_\beta\right)^2\left(\mathcal{D}\varepsilon(G)\right)\Big\vert_{\alpha=1,\beta=1}$

In Table 2,

$$\partial_\alpha f(\alpha,\beta) = \alpha\frac{\partial(f(\alpha,\beta))}{\partial\alpha}, \qquad \partial_\beta f(\alpha,\beta) = \beta\frac{\partial(f(\alpha,\beta))}{\partial\beta}$$

The chemical structures (molecular graphs) of the drugs which we have considered in this paper are given in Figures 2 to 5.

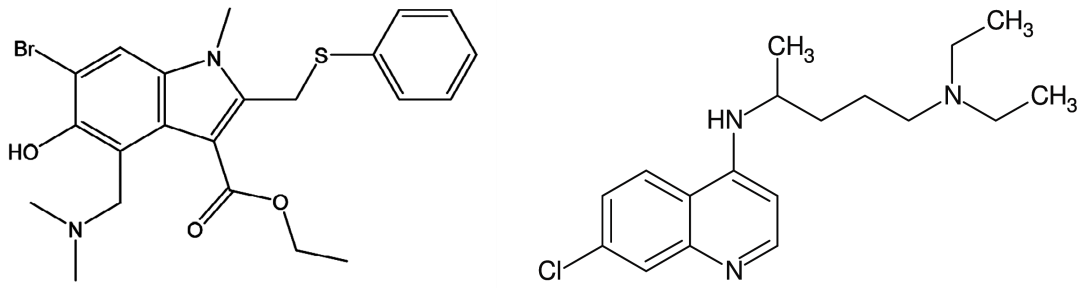

Figure 2. Molecular graphs of Arbidol and Chloroquine.

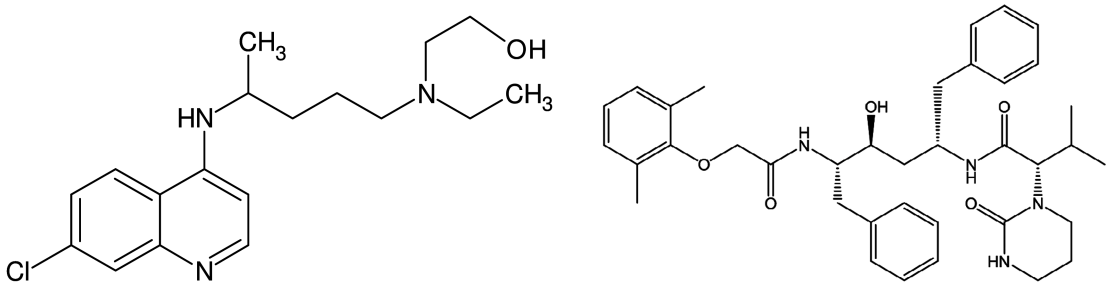

Figure 3. Molecular graphs of Hydroxy-chloroquine and Lopinavir.

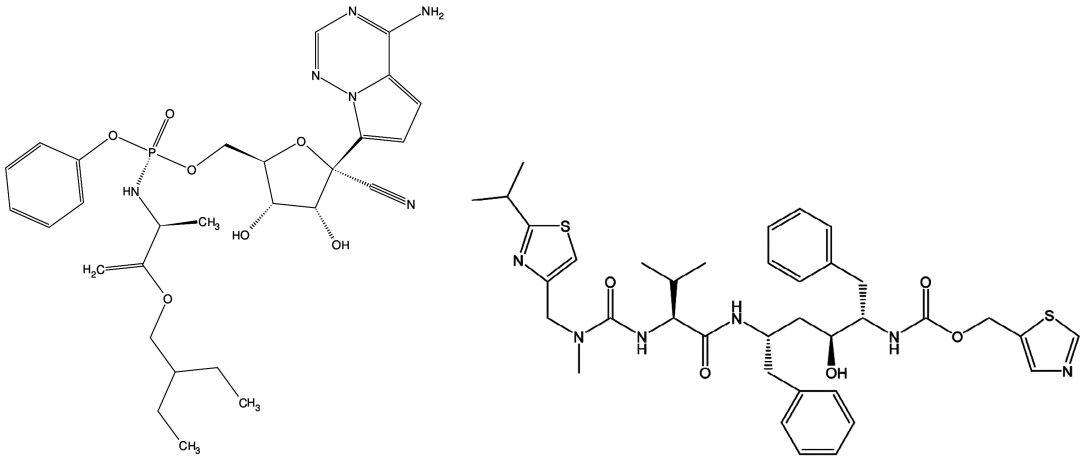

Figure 4. Molecular Graphs of Remdesivir and Ritonavir.

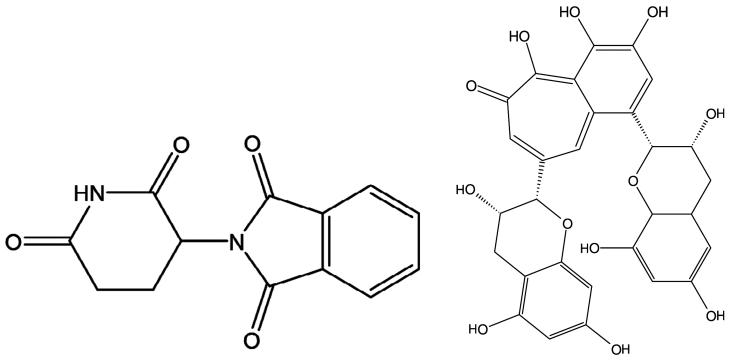

Figure 5. Molecular graphs of Thalidomide and Theaflavin.

2. Methodology

We use the method of edge partitions and the newly introduced $\mathcal{D}\varepsilon$-polynomial to compute our proposed indices. Edge partitioning is the process of grouping (partitioning) edges based on the appropriate vertex degrees of the end vertices of the edges of a graph. By "appropriate", we refer to the type of vertex degrees used to compute the topological indices. For example, in order to partition the edges for computing our proposed indices, we make use of the diameter eccentricity based vertex degrees of the end vertices of the edges.

In Tables 3 to 10, we present the distance eccentricity based edge partitions for the eight COVID-19 drugs. Here, $r\rho_{(p,q)}$ is the number of edges in the edge partition $(d\varepsilon_p, d\varepsilon_q)$ in a graph G.

Table 3. $d\varepsilon-$edge partitions of Arbidol A.

$(d\varepsilon_p, d\varepsilon_q)$:	$(1,2)$	$(2,3)$	$(3,3)$	$(3,4)$	$(4,5)$	$(5,5)$	$(5,6)$	$(6,7)$
$r\rho_{(p,q)}$:	4	6	1	6	5	1	5	3

From Table 3 we observe that the edges of Arbidol can be partitioned into 8 partitions based on the distance eccentricity based vertex degrees of the end vertices of the edges of the molecular graph of Arbidol.

Table 4. $d\varepsilon-$edge partitions of Chloroquine C.

$(d\varepsilon_p, d\varepsilon_q)$:	$(1,2)$	$(2,3)$	$(3,4)$	$(4,5)$	$(5,6)$	$(6,7)$	$(7,7)$
$r\rho_{(p,q)}$:	3	4	5	4	3	3	1

From Table 4 we observe that the edges of Chloroquine can be partitioned into 7 partitions based on the distance eccentricity based vertex degrees of the end vertices of the edges of the molecular graph of Chloroquine.

Table 5. $d\varepsilon-$edge partitions of Hydroxy-Chloroquine HC.

$(d\varepsilon_p, d\varepsilon_q)$:	$(1,2)$	$(2,3)$	$(3,4)$	$(4,5)$	$(5,6)$	$(6,7)$	$(7,8)$
$r\rho_{(p,q)}$:	2	4	6	4	3	2	3

From Table 5 we observe that the edges of Hydroxy-Chloroquine can be partitioned into 7 partitions based on the distance eccentricity based vertex degrees of the end vertices of the edges of the molecular graph of Hydroxy-Chloroquine.

Table 6. $d\varepsilon-$edge partitions of Lopinavir L.

$(d\varepsilon_p, d\varepsilon_q)$:	$(1,2)$	$(2,3)$	$(3,4)$	$(4,5)$	$(5,6)$	$(6,7)$	$(7,8)$	$(8,9)$	$(9,10)$
$r\rho_{(p,q)}$:	5	6	8	7	7	6	4	3	3

From Table 6 we observe that the edges of Lopinavir can be partitioned into 9 partitions based on the distance eccentricity based vertex degrees of the end vertices of the edges of the molecular graph of Lopinavir.

Table 7. $d\varepsilon-$edge partitions of Remdesivir R.

$(d\varepsilon_p, d\varepsilon_q)$:	$(1,2)$	$(2,3)$	$(3,3)$	$(3,4)$	$(4,5)$	$(5,6)$	$(6,6)$	$(6,7)$	$(7,8)$	$(8,9)$	$(9,10)$
$r\rho_{(p,q)}$:	5	4	1	4	5	7	1	7	4	4	2

From Table 7 we observe that the edges of Remdesivir can be partitioned into 11 partitions based on the distance eccentricity based vertex degrees of the end vertices of the edges of the molecular graph of Remdesivir.

Table 8. $d\varepsilon-$edge partitions of Ritonavir Ri.

$(d\varepsilon_p, d\varepsilon_q)$:	$(1,1)$	$(1,2)$	$(2,3)$	$(3,3)$	$(3,4)$	$(4,5)$	$(5,6)$	$(6,7)$	$(7,8)$	$(8,9)$	$(9,10)$	$(10,11)$	$(11,12)$
$r\rho_{(p,q)}$:	1	4	3	1	5	5	5	6	6	7	4	4	2

From Table 8 we observe that the edges of Ritonavir can be partitioned into 13 partitions based on the distance eccentricity based vertex degrees of the end vertices of the edges of the molecular graph of Ritonavir.

Table 9. $d\varepsilon-$edge partitions of Thalidomide T.

$(d\varepsilon_p, d\varepsilon_q)$:	$(1,1)$	$(1,2)$	$(2,3)$	$(3,3)$	$(3,4)$	$(4,5)$	$(5,5)$
$r\rho_{(p,q)}$:	1	3	4	1	7	4	1

From Table 9 we observe that the edges of Thalidomide can be partitioned into 7 partitions based on the distance eccentricity based vertex degrees of the end vertices of the edges of the molecular graph of Thalidomide.

Table 10. $d\varepsilon-$edge partitions of Theaflavin Th.

$(d\varepsilon_p, d\varepsilon_q)$:	$(1,2)$	$(2,3)$	$(3,4)$	$(4,5)$	$(5,6)$	$(6,6)$	$(6,7)$	$(7,7)$	$(7,8)$	$(8,8)$
$r\rho_{(p,q)}$:	8	4	6	7	8	1	7	1	3	1

From Table 10 we observe that the edges of Theaflavin can be partitioned into 10 partitions based on the distance eccentricity based vertex degrees of the end vertices of the edges of the molecular graph of Theaflavin.

3. Main results

In this section, we compute $\mathcal{D}\varepsilon$-polynomial of the molecular graphs of the mentioned COVID-19 drugs and obtain our proposed topological indices values.

3.1. $\mathcal{D}\varepsilon$-polynomial and $\mathcal{D}\varepsilon$ Indices for Arbidol

Theorem 3.1. *Let A be the molecular graph of Arbidol. Then, we have,*

$$\mathcal{D}\varepsilon(A) = 4\alpha^1\beta^2 + 6\alpha^2\beta^3 + \alpha^3\beta^3 + 6\alpha^3\beta^4 + 5\alpha^4\beta^5 + \alpha^5\beta^5 + 5\alpha^5\beta^6 + 3\alpha^6\beta^7.$$

Proof. Let A be the molecular graph of Arbidol represented in Figure 2. It has 29 vertices and 31 edges. Consider

$$\begin{aligned}\mathcal{D}\varepsilon(A) &= \sum_{i\leq j}(r\rho_{(i,j)})\alpha^i\beta^j \\ &= r\rho_{(1,2)}\alpha^1\beta^2 + r\rho_{(2,3)}\alpha^2\beta^3 + r\rho_{(3,3)}\alpha^3\beta^3 + r\rho_{(3,4)}\alpha^3\beta^4 + r\rho_{(4,5)}\alpha^4\beta^5 + r\rho_{(5,5)}\alpha^5\beta^5 \\ &+ r\rho_{(5,6)}\alpha^5\beta^6 + r\rho_{(6,7)}\alpha^6\beta^7.\end{aligned}$$

Using the edge partitions given in Table 3, it is clear that $r\rho_{(1,2)} = 4$, $r\rho_{(2,3)} = 6$, $r\rho_{(3,3)} = 1$, $r\rho_{(3,4)} = 6$, $r\rho_{(4,5)} = 5$, $r\rho_{(5,5)} = 1$, $r\rho_{(5,6)} = 5$ and $r\rho_{(6,7)} = 3$.

Applying these values in $\mathcal{D}\varepsilon(A)$, we get the $\mathcal{D}\varepsilon$-polynomial for Arbidol as follows:

$$\mathcal{D}\varepsilon(A) = 4\alpha^1\beta^2 + 6\alpha^2\beta^3 + \alpha^3\beta^3 + 6\alpha^3\beta^4 + 5\alpha^4\beta^5 + \alpha^5\beta^5 + 5\alpha^5\beta^6 + 3\alpha^6\beta^7.$$

□

Proposition 3.2. *Let A be the molecular graph of Arbidol. Then, we have,*

1) $\mathcal{D}R_1\varepsilon(A) = 239$.
2) $\mathcal{D}R_2\varepsilon(A) = 546$.
3) $H\mathcal{D}R_1\varepsilon(A) = 2133$.
4) $H\mathcal{D}R_2\varepsilon(A) = 13594$.

Proof. Using the derivation formula given in Table 2 and the $\mathcal{D}\varepsilon$-polynomial for Arbidol from Theorem 3.1, we have

$$\begin{aligned}
\mathcal{D}R_1\varepsilon(A) &= \Big(\partial_\alpha + \partial_\beta\Big)\Big(\mathcal{D}\varepsilon(A)\Big)\Big|_{\alpha=\beta=1} \\
&= \Big(\partial_\alpha \mathcal{D}\varepsilon(A) + \partial_\beta \mathcal{D}\varepsilon(A)\Big)\Big|_{\alpha=\beta=1} = \Big(\partial_\alpha\Big(f(\alpha,\beta)\Big) + \partial_\beta\Big(f(\alpha,\beta)\Big)\Big)|_{\alpha=\beta=1} \\
&= \Big(\Big(\alpha\frac{\partial\Big(4\alpha^1\beta^2 + 6\alpha^2\beta^3 + \alpha^3\beta^3 + 6\alpha^3\beta^4 + 5\alpha^4\beta^5 + \alpha^5\beta^5 + 5\alpha^5\beta^6 + 3\alpha^6\beta^7\Big)}{\partial\alpha}\Big) \\
&\quad + \Big(\beta\frac{\partial\Big(4\alpha^1\beta^2 + 6\alpha^2\beta^3 + \alpha^3\beta^3 + 6\alpha^3\beta^4 + 5\alpha^4\beta^5 + \alpha^5\beta^5 + 5\alpha^5\beta^6 + 3\alpha^6\beta^7\Big)}{\partial\beta}\Big)\Big)\Big|_{\alpha=\beta=1} \\
&= \Big(12\alpha^1\beta^2 + 30\alpha^2\beta^3 + 6\alpha^3\beta^3 + 42\alpha^3\beta^4 + 10\alpha^4\beta^5 + \alpha^5\beta^5 + 55\alpha^5\beta^6 + 39\alpha^6\beta^7\Big)\Big|_{\alpha=\beta=1} = 239.
\end{aligned}$$

Similarly, the other three indices can be obtained as follows:

$$\begin{aligned}
\mathcal{D}R_2\varepsilon(A) &= \Big(\partial_\alpha * \partial_\beta\Big)\Big(\mathcal{D}\varepsilon(A)\Big)\Big|_{\alpha=\beta=1} = \Big(\partial_\alpha * \partial_\beta\Big)\Big(f(\alpha,\beta)\Big)\Big|_{\alpha=\beta=1} \\
&= \Big(8\alpha^1\beta^2 + 36\alpha^2\beta^3 + 9\alpha^3\beta^3 + 72\alpha^3\beta^4 + 120\alpha^4\beta^5 + 25\alpha^5\beta^5 + 150\alpha^5\beta^6 + 126\alpha^6\beta^7\Big)\Big|_{\alpha=\beta=1} = 546.
\end{aligned}$$

$$\begin{aligned}
H\mathcal{D}R_1\varepsilon(A) &= \Big(\partial_\alpha + \partial_\beta\Big)^2\Big(\mathcal{D}\varepsilon(A)\Big)\Big|_{\alpha=\beta=1} = \Big(\partial_\alpha + \partial_\beta\Big)^2\Big(f(\alpha,\beta)\Big)\Big|_{\alpha=\beta=1} \\
&= \Big(36\alpha^1\beta^2 + 150\alpha^2\beta^3 + 36\alpha^3\beta^3 + 294\alpha^3\beta^4 + 405\alpha^4\beta^5 + 100\alpha^5\beta^5 + 605\alpha^5\beta^6 + 507\alpha^6\beta^7\Big)\Big|_{\alpha=\beta=1} = 2133.
\end{aligned}$$

$$\begin{aligned}
H\mathcal{D}R_2\varepsilon(A) &= \Big(\partial_\alpha * \partial_\beta\Big)^2\Big(\mathcal{D}\varepsilon(A)\Big)\Big|_{\alpha=\beta=1} = \Big(\partial_\alpha * \partial_\beta\Big)^2\Big(f(\alpha,\beta)\Big)\Big|_{\alpha=\beta=1} \\
&= \Big(16\alpha^1\beta^2 + 216\alpha^2\beta^3 + 81\alpha^3\beta^3 + 864\alpha^3\beta^4 + 2000\alpha^4\beta^5 + 625\alpha^5\beta^5 + 4500\alpha^5\beta^6 + 5292\alpha^6\beta^7\Big)\Big|_{\alpha=\beta=1} = 13594.
\end{aligned}$$

□

3.2. $\mathcal{D}\varepsilon$-polynomial and $\mathcal{D}\varepsilon$ Indices for Chloroquine

Theorem 3.3. *Let C be the molecular graph of Chloroquine. Then, we have,*

$$\mathcal{D}\varepsilon(C) = 3\alpha^1\beta^2 + 4\alpha^2\beta^3 + 5\alpha^3\beta^4 + 4\alpha^4\beta^5 + 3\alpha^5\beta^6 + 3\alpha^6\beta^7 + \alpha^7\beta^7.$$

Proof. Let C be the molecular graph of Chloroquine represented in Figure 2. It has 21 vertices and 23 edges. Consider

$$\begin{aligned}\mathcal{D}\varepsilon(C) &= \sum_{i\leq j}(r\rho_{(i,j)})\alpha^i\beta^j \\ &= r\rho_{(1,2)}\alpha^1\beta^2 + r\rho_{(2,3)}\alpha^2\beta^3 + r\rho_{(3,4)}\alpha^3\beta^4 + r\rho_{(4,5)}\alpha^4\beta^5 + r\rho_{(5,6)}\alpha^5\beta^6 \\ &+ r\rho_{(6,7)}\alpha^6\beta^7 + r\rho_{(7,7)}\alpha^7\beta^7.\end{aligned}$$

Using the edge partitions given in Table 4, it is clear that $r\rho_{(1,2)} = 3$, $r\rho_{(2,3)} = 4$, $r\rho_{(3,4)} = 5$, $r\rho_{(4,5)} = 4$, $r\rho_{(5,6)} = 3$, $r\rho_{(6,7)} = 3$ and $r\rho_{(7,7)} = 1$.

Applying the values in $\mathcal{D}\varepsilon(C)$, we get the $\mathcal{D}\varepsilon$-polynomial for Chloroquine as follows:

$$\mathcal{D}\varepsilon(C) = 3\alpha^1\beta^2 + 4\alpha^2\beta^3 + 5\alpha^3\beta^4 + 4\alpha^4\beta^5 + 3\alpha^5\beta^6 + 3\alpha^6\beta^7 + \alpha^7\beta^7.$$

□

Proposition 3.4. *Let C be the molecular graph of Chloroquine. Then, we have,*

1) $\mathcal{D}R_1\varepsilon(C) = 186$.
2) $\mathcal{D}R_2\varepsilon(C) = 435$.
3) $H\mathcal{D}R_1\varepsilon(C) = 1762$.
4) $H\mathcal{D}R_2\varepsilon(C) = 12869$.

Proof is similar to that of proposition 3.2.

3.3. $\mathcal{D}\varepsilon$-polynomial and $\mathcal{D}\varepsilon$ Indices for Hydroxy-Chloroquine

Theorem 3.5. *Let HC be the molecular graph of Hydroxy-Chloroquine. Then, we have,*

$$\mathcal{D}\varepsilon(HC) = 2\alpha^1\beta^2 + 4\alpha^2\beta^3 + 6\alpha^3\beta^4 + 4\alpha^4\beta^5 + 3\alpha^5\beta^6 + 2\alpha^6\beta^7 + 3\alpha^7\beta^8.$$

Proof. Let HC be the molecular graph of Hydroxy-Chloroquine represented in Figure 3. It has 22 vertices and 24 edges. Consider

$$\begin{aligned}\mathcal{D}\varepsilon(HC) &= \sum_{i\leq j}(r\rho_{(i,j)})\alpha^i\beta^j \\ &= r\rho_{(1,2)}\alpha^1\beta^2 + r\rho_{(2,3)}\alpha^2\beta^3 + r\rho_{(3,4)}\alpha^3\beta^4 + r\rho_{(4,5)}\alpha^4\beta^5 + r\rho_{(5,6)}\alpha^5\beta^6 \\ &+ r\rho_{(6,7)}\alpha^6\beta^7 + r\rho_{(7,8)}\alpha^7\beta^8.\end{aligned}$$

Using the edge partitions given in Table 5, it is clear that $r\rho_{(1,2)} = 2$, $r\rho_{(2,3)} = 4$, $r\rho_{(3,4)} = 6$, $r\rho_{(4,5)} = 4$, $r\rho_{(5,6)} = 3$, $r\rho_{(6,7)} = 2$ and $r\rho_{(7,8)} = 3$.

Applying the values in $\mathcal{D}\varepsilon(HC)$, we get the $\mathcal{D}\varepsilon$-polynomial for Hydroxy-Chloroquine as follows:

$$\mathcal{D}\varepsilon(HC) = 2\alpha^1\beta^2 + 4\alpha^2\beta^3 + 6\alpha^3\beta^4 + 4\alpha^4\beta^5 + 3\alpha^5\beta^6 + 2\alpha^6\beta^7 + 3\alpha^7\beta^8.$$

□

Proposition 3.6. *Let HC be the molecular graph of Hydroxy-Chloroquine. Then, we have,*

1) $\mathcal{D}R_1\varepsilon(HC) = 208$.
2) $\mathcal{D}R_2\varepsilon(HC) = 522$.
3) $H\mathcal{D}R_1\varepsilon(HC) = 2092$.
4) $H\mathcal{D}R_2\varepsilon(HC) = 18252$.

Proof is similar to that of proposition 3.2.

3.4. $\mathcal{D}\varepsilon$-polynomial and $\mathcal{D}\varepsilon$ Indices for Lopinavir

Theorem 3.7. *Let L be the molecular graph of Lopinavir. Then, we have,*

$$\mathcal{D}\varepsilon(L) = 5\alpha^1\beta^2 + 6\alpha^2\beta^3 + 8\alpha^3\beta^4 + 7\alpha^4\beta^5 + 7\alpha^5\beta^6 + 6\alpha^6\beta^7 + 4\alpha^7\beta^8.$$

Proof. Let L be the molecular graph of Lopinavir represented in Figure 3. It has 46 vertices and 49 edges. Consider

$$\begin{aligned}\mathcal{D}\varepsilon(L) &= \sum_{i\leq j}(r\rho_{(i,j)})\alpha^i\beta^j \\ &= r\rho_{(1,2)}\alpha^1\beta^2 + r\rho_{(2,3)}\alpha^2\beta^3 + r\rho_{(3,4)}\alpha^3\beta^4 + r\rho_{(4,5)}\alpha^4\beta^5 + r\rho_{(5,6)}\alpha^5\beta^6 \\ &+ r\rho_{(6,7)}\alpha^6\beta^7 + r\rho_{(7,8)}\alpha^7\beta^8.\end{aligned}$$

Using the edge partitions given in Table 6, it is clear that $r\rho_{(1,2)} = 5$, $r\rho_{(2,3)} = 6$, $r\rho_{(3,4)} = 8$, $r\rho_{(4,5)} = 7$, $r\rho_{(5,6)} = 7$, $r\rho_{(6,7)} = 6$ and $r\rho_{(7,8)} = 4$.

Applying the values in $\mathcal{D}\varepsilon(L)$, we get the $\mathcal{D}\varepsilon$-polynomial for Lopinavir as follows:

$$\mathcal{D}\varepsilon(L) = 5\alpha^1\beta^2 + 6\alpha^2\beta^3 + 8\alpha^3\beta^4 + 7\alpha^4\beta^5 + 7\alpha^5\beta^6 + 6\alpha^6\beta^7 + 4\alpha^7\beta^8.$$

□

Proposition 3.8. *Let L be the molecular graph of Lopinavir. Then, we have,*

1) $\mathcal{D}R_1\varepsilon(L) = 487$.
2) $\mathcal{D}R_2\varepsilon(L) = 1454$.
3) $H\mathcal{D}R_1\varepsilon(L) = 5865$.
4) $H\mathcal{D}R_2\varepsilon(L) = 73468$.

Proof is similar to that of proposition 3.2.

3.5. $\mathcal{D}\varepsilon$-polynomial and $\mathcal{D}\varepsilon$ Indices for Remdesivir

Theorem 3.9. *Let R be the molecular graph of Remdesivir. Then, we have,*

$$\mathcal{D}\varepsilon(R) = 5\alpha^1\beta^2 + 4\alpha^2\beta^3 + 1\alpha^3\beta^3 + 4\alpha^3\beta^4 + 5\alpha^4\beta^5 + 7\alpha^5\beta^6 + 1\alpha^6\beta^6 + 7\alpha^6\beta^7 + 4\alpha^7\beta^8 + 4\alpha^8\beta^9 + 2\alpha^9\beta^{10}.$$

Proof. Let R be the molecular graph of Remdesivir represented in Figure 4. It has 41 vertices and 44 edges. Consider

$$\begin{aligned}\mathcal{D}\varepsilon(R) &= \sum_{i\leq j}(r\rho_{(i,j)})\alpha^i\beta^j \\ &= r\rho_{(1,2)}\alpha^1\beta^2 + r\rho_{(2,3)}\alpha^2\beta^3 + r\rho_{(3,3)}\alpha^3\beta^3 + r\rho_{(3,4)}\alpha^3\beta^4 + r\rho_{(4,5)}\alpha^4\beta^5 + r\rho_{(5,6)}\alpha^5\beta^6 \\ &+ r\rho_{(6,6)}\alpha^6\beta^6 + r\rho_{(6,7)}\alpha^6\beta^7 + r\rho_{(7,8)}\alpha^7\beta^8 + r\rho_{(8,9)}\alpha^8\beta^9 + r\rho_{(9,19)}\alpha^9\beta^{10}.\end{aligned}$$

Using the edge partitions given in Table 7, it is clear that $r\rho_{(1,2)} = 5$, $r\rho_{(2,3)} = 4$, $r\rho_{(3,3)} = 1$, $r\rho_{(3,4)} = 4$, $r\rho_{(4,5)} = 5$, $r\rho_{(5,6)} = 7$, $r\rho_{(6,6)} = 1$, $r\rho_{(6,7)} = 7$, $r\rho_{(7,8)} = 4$, $r\rho_{(8,9)} = 4$ and $r\rho_{(9,10)} = 2$.

Applying the values in $\mathcal{D}\varepsilon(R)$, we get the $\mathcal{D}\varepsilon$-polynomial for Remdesivir as follows:

$$\mathcal{D}\varepsilon(R) = 5\alpha^1\beta^2 + 4\alpha^2\beta^3 + 1\alpha^3\beta^3 + 4\alpha^3\beta^4 + 5\alpha^4\beta^5 + 7\alpha^5\beta^6 + 1\alpha^6\beta^6 + 7\alpha^6\beta^7 + 4\alpha^7\beta^8 + 4\alpha^8\beta^9 + 2\alpha^9\beta^{10}.$$

□

Proposition 3.10. *Let R be the molecular graph of Remdesivir. Then, we have,*

1) $\mathcal{D}R_1\varepsilon(R) = 460$.
2) $\mathcal{D}R_2\varepsilon(R) = 1423$.
3) $H\mathcal{D}R_1\varepsilon(R) = 5734$.
4) $H\mathcal{D}R_2\varepsilon(R) = 72245$.

Proof is similar to that of proposition 3.2.

3.6. $\mathcal{D}\varepsilon$-polynomial and $\mathcal{D}\varepsilon$ Indices for Ritonavir

Theorem 3.11. *Let Ri be the molecular graph of Ritonavir. Then, we have,*

$$\begin{aligned}\mathcal{D}\varepsilon(Ri) &= 1\alpha^1\beta^1 + 4\alpha^1\beta^2 + 3\alpha^2\beta^3 + 1\alpha^3\beta^3 + 5\alpha^3\beta^4 + 5\alpha^4\beta^5 + 5\alpha^5\beta^6 + 6\alpha^6\beta^7 + 6\alpha^7\beta^8 \\ &+ 7\alpha^8\beta^9 + 4\alpha^9\beta^{10} + 4\alpha^{10}\beta^{11} + 2\alpha^{11}\beta^{12}.\end{aligned}$$

Proof. Let Ri be the molecular graph of Ritonavir represented in Figure 4. It has 50 vertices and 53 edges. Consider

$$\begin{aligned}\mathcal{D}\varepsilon(Ri) &= \sum_{i\leq j}(r\rho_{(i,j)})\alpha^i\beta^j \\ &= r\rho_{(1,1)}\alpha^1\beta^1 + r\rho_{(1,2)}\alpha^1\beta^2 + r\rho_{(2,3)}\alpha^2\beta^3 + r\rho_{(3,3)}\alpha^3\beta^3 + r\rho_{(3,4)}\alpha^3\beta^4 + r\rho_{(4,5)}\alpha^4\beta^5 + r\rho_{(5,6)}\alpha^5\beta^6 \\ &+ r\rho_{(6,7)}\alpha^6\beta^7 + r\rho_{(7,8)}\alpha^7\beta^8 + r\rho_{(8,9)}\alpha^8\beta^9 + r\rho_{(9,10)}\alpha^9\beta^{10} + r\rho_{(10,11)}\alpha^{10}\beta^{11} + r\rho_{(11,12)}\alpha^{11}\beta^{12}.\end{aligned}$$

Using the edge partitions given in Table 8, it is clear that $r\rho_{(1,1)} = 1$, $r\rho_{(1,2)} = 4$, $r\rho_{(2,3)} = 3$, $r\rho_{(3,3)} = 1$, $r\rho_{(3,4)} = 5$, $r\rho_{(4,5)} = 5$, $r\rho_{(5,6)} = 5$, $r\rho_{(6,7)} = 6$, $r\rho_{(7,8)} = 6$, $r\rho_{(8,9)} = 7$, $r\rho_{(9,10)} = 4$, $r\rho_{(10,11)} = 4$, $r\rho_{11,12)} = 2$.

Applying the values in $\mathcal{D}\varepsilon(Ri)$, we get the $\mathcal{D}\varepsilon$-polynomial for Ritonavir as follows:

$$\mathcal{D}\varepsilon(Ri) = 1\alpha^1\beta^1 + 4\alpha^1\beta^2 + 3\alpha^2\beta^3 + 1\alpha^3\beta^3 + 5\alpha^3\beta^4 + 5\alpha^4\beta^5 + 5\alpha^5\beta^6 + 6\alpha^6\beta^7 + 6\alpha^7\beta^8 + 7\alpha^8\beta^9 + 4\alpha^9\beta^{10} + 4\alpha^{10}\beta^{11} + 2\alpha^{11}\beta^{12}.$$

□

Proposition 3.12. *Let Ri be the molecular graph of Ritonavir. Then, we have,*

1) $\mathcal{D}R_1\varepsilon(Ri) = 629$.
2) $\mathcal{D}R_2\varepsilon(Ri) = 2502$.
3) $H\mathcal{D}R_1\varepsilon(Ri) = 10059$.
4) $H\mathcal{D}R_2\varepsilon(Ri) = 188762$.

Proof is similar to that of proposition 3.2.

3.7. $\mathcal{D}\varepsilon$-polynomial and $\mathcal{D}\varepsilon$ Indices for Thalidomide

Theorem 3.13. *Let T be the molecular graph of Thalidomide. Then, we have,*

$$\mathcal{D}\varepsilon(T) = 1\alpha^1\beta^1 + 3\alpha^1\beta^2 + 4\alpha^2\beta^3 + 1\alpha^3\beta^3 + 7\alpha^3\beta^4 + 4\alpha^4\beta^5 + 1\alpha^5\beta^5.$$

Proof. Let T be the molecular graph of Thalidomide represented in Figure 5. It has 19 vertices and 21 edges. Consider

$$\begin{aligned}\mathcal{D}\varepsilon(T) &= \sum_{i\leq j}(r\rho_{(i,j)})\alpha^i\beta^j \\ &= r\rho_{(1,1)}\alpha^1\beta^1 + r\rho_{(1,2)}\alpha^1\beta^2 + r\rho_{(2,3)}\alpha^2\beta^3 + r\rho_{(3,3)}\alpha^3\beta^3 + r\rho_{(3,4)}\alpha^3\beta^4 + r\rho_{(4,5)}\alpha^4\beta^5 + r\rho_{(5,5)}\alpha^5\beta^5.\end{aligned}$$

Using the edge partitions given in Table 9, it is clear that $r\rho_{(1,1)} = 1$, $r\rho_{(1,2)} = 3$, $r\rho_{(2,3)} = 4$, $r\rho_{(3,3)} = 1$, $r\rho_{(3,4)} = 7$, $r\rho_{(4,5)} = 4$ and $r\rho_{(5,5)} = 1$.

Applying the values in $\mathcal{D}\varepsilon(T)$, we get the $\mathcal{D}\varepsilon$-polynomial for Thalidomide as follows:

$$\mathcal{D}\varepsilon(T) = 1\alpha^1\beta^1 + 3\alpha^1\beta^2 + 4\alpha^2\beta^3 + 1\alpha^3\beta^3 + 7\alpha^3\beta^4 + 4\alpha^4\beta^5 + 1\alpha^5\beta^5.$$

□

Proposition 3.14. *Let T be the molecular graph of Thalidomide. Then, we have,*

1) $\mathcal{D}R_1\varepsilon(T) = 132$.
2) $\mathcal{D}R_2\varepsilon(T) = 229$.
3) $H\mathcal{D}R_1\varepsilon(T) = 934$.
4) $H\mathcal{D}R_2\varepsilon(T) = 3471$.

Proof is similar to that of proposition 3.2.

3.8. $\mathcal{D}\varepsilon$-polynomial and $\mathcal{D}\varepsilon$ indices for Theaflavin

Theorem 3.15. *Let Th be the molecular graph of Theaflavin. Then, we have,*

$$\mathcal{D}\varepsilon(Th) = 8\alpha^1\beta^2 + 4\alpha^2\beta^3 + 6\alpha^3\beta^4 + 7\alpha^4\beta^5 + 8\alpha^5\beta^6 + 1\alpha^6\beta^6 + 7\alpha^6\beta^7 + 1\alpha^7\beta^7 + 3\alpha^7\beta^8 + 1\alpha^8\beta^8.$$

Proof. Let Th be the molecular graph of Theaflavin represented in Figure 5. It has 41 vertices and 46 edges. Consider

$$\begin{aligned}\mathcal{D}\varepsilon(Th) &= \sum_{i\leq j}(r\rho_{(i,j)})\alpha^i\beta^j \\ &= r\rho_{(1,2)}\alpha^1\beta^2 + r\rho_{(2,3)}\alpha^2\beta^3 + r\rho_{(3,4)}\alpha^3\beta^4 + r\rho_{(4,5)}\alpha^4\beta^5 + r\rho_{(5,6)}\alpha^5\beta^6 + r\rho_{(6,6)}\alpha^6\beta^6 \\ &+ r\rho_{(6,7)}\alpha^6\beta^7 + r\rho_{(7,7)}\alpha^7\beta^7 + r\rho_{(7,8)}\alpha^7\beta^8 + r\rho_{(8,8)}\alpha^8\beta^8.\end{aligned}$$

Using the edge partitions given in Table 10, it is clear that $r\rho_{(1,2)} = 8$, $r\rho_{(2,3)} = 4$, $r\rho_{(3,4)} = 6$, $r\rho_{(4,5)} = 7$, $r\rho_{(5,6)} = 8$, $r\rho_{(6,6)} = 1$, $r\rho_{(6,7)} = 7$, $r\rho_{(7,7)} = 1$, $r\rho_{(7,8)} = 3$ and $r\rho_{(8,8)} = 1$.

Applying the values in $\mathcal{D}\varepsilon(Th)$, we get the $\mathcal{D}\varepsilon$-polynomial for Theaflavin as follows:

$$\mathcal{D}\varepsilon(Th) = 8\alpha^1\beta^2 + 4\alpha^2\beta^3 + 6\alpha^3\beta^4 + 7\alpha^4\beta^5 + 8\alpha^5\beta^6 + 1\alpha^6\beta^6 + 7\alpha^6\beta^7 + 1\alpha^7\beta^7 + 3\alpha^7\beta^8 + 1\alpha^8\beta^8.$$

□

Proposition 3.16. *Let Th be the molecular graph of Theaflavin. Then, we have,*

1) $\mathcal{D}R_1\varepsilon(Th) = 415$.
2) $\mathcal{D}R_2\varepsilon(Th) = 1103$.
3) $H\mathcal{D}R_1\varepsilon(Th) = 3944$.
4) $H\mathcal{D}R_2\varepsilon(Th) = 40589$.

Proof is similar to that of proposition 3.2.

4. Curvilinear regression analysis of COVID-19 drugs

In this section, we analyze the topological indices given in Table 1 for the following physico-chemical properties of the 8 COVID-19 antiviral drugs: Boiling point (BP), Enthalpy (E), Flash point (FP), Molar refraction (MR), Polar Surface Area (PSA), Polarizability (P), Surface Tension (T), Molar Volume (MV).

Experimental values of physico-chemical properties of the antiviral drugs presented in Table 11 were obtained from Kirmani et al. [22]. In Table 12 we have presented the values of the proposed indices calculated in Section 3.

Table 11. Physico-chemical properties of COVID-19 drugs.

Drugs	BP	E	FP	MR	PSA	P	T	MV
Arbidol	591.8	91.5	311.7	121.9	80	48.3	45.3	347.3
Chloroquine	460.6	72.1	232.3	97.4	28	38.6	44	287.9
Hydroxy-Chloroquine	516.7	83	266.3	99	48	39.2	49.8	285.4
Lopinavir	924.2	140.8	512.7	179.2	120	71	49.5	540.5
Remdesivir	-	-	-	149.5	213	59.3	62.3	409
Ritonavir	947	144.4	526.6	198.9	202	78.9	53.7	581.7
Thalidomide	487.8	79.4	248.8	65.2	87	25.9	71.6	161
Theaflavin	1003.9	153.5	336.5	137.3	218	54.4	138.6	301

Table 12. Topological descriptor values of COVID-19 drugs.

Drugs	$\mathcal{D}R_1\varepsilon$	$\mathcal{D}R_2\varepsilon$	$H\mathcal{D}R_1\varepsilon$	$H\mathcal{D}R_2\varepsilon$
Arbidol	239	546	2133	13594
Chloroquine	186	435	1762	12869
Hydroxy-Chloroquine	208	522	2092	18252
Lopinavir	487	1454	5865	73468
Remdesivir	460	1423	5734	72245
Ritonavir	629	2502	10059	188762
Thalidomide	132	229	934	3471
Theaflavin	415	1103	3944	40589

We performed curvilinear regression analysis for our proposed indices aganist the physico-chemical properties.
The general form of the curvilinear regression model is

$$P = \left[\sum_{i=1}^{n} \tilde{\alpha}_i (TI)^i\right] + \tilde{\gamma} \tag{4.1}$$

where P is the physico-chemical property (dependent variable), $\tilde{\gamma}$ is the regression model constant, and $\tilde{\alpha}_i$ are the coefficients corresponding to topological descriptors (TI), $i = 1, 2, \ldots, n$.

We performed a comparative analysis of the linear, quadratic, cubic and fourth order curvilinear regression models. The models for which $R^2 \geq 0.8$ (as per International Academy of Mathematical Chemistry Guidelines) were considered for further analysis. We observed the following:

- From Table 13, it can be seen that the R^2 values for the following properties: boiling point (BP), enthalpy (E), flash point (FP), molar refraction (MR), polarizability (P) and molar volume (MV), are higher for the cubic models and they can be used to predict these properties. However, polar surface area (PSA) and surface tension (T) could not be predicted using the cubic models.
- All the eight physico-chemical properties could be predicted using fourth order regression models.

Table 13. Predictive fits from linear, quadratic and cubic regression models.

Property	Linear	R^2	$RMSE$	Quadratic	R^2	$RMSE$	Cubic	R^2	$RMSE$
BP	$\mathcal{D}R_1\varepsilon$	0.8273	110.1231	$\mathcal{D}R_1\varepsilon$	0.9112	88.2792	$\mathcal{D}R_1\varepsilon$	0.9494	76.9536
E	$\mathcal{D}R_1\varepsilon$	0.8170	16.5276	$\mathcal{D}R_1\varepsilon$	0.8965	13.8998	$\mathcal{D}R_1\varepsilon$	0.9413	12.0807
FP	$\mathcal{D}R_1\varepsilon$	0.8851	45.5738	$H\mathcal{D}R_2\varepsilon$	0.9200	42.5140	$H\mathcal{D}R_2\varepsilon$	0.9625	33.5907
MR	$\mathcal{D}R_1\varepsilon$	0.9356	12.2073	$\mathcal{D}R_1\varepsilon$	0.9377	13.1566	$\mathcal{D}R_1\varepsilon$	0.9551	12.4885
P	$\mathcal{D}R_1\varepsilon$	0.9363	4.8138	$\mathcal{D}R_1\varepsilon$	0.9382	5.1930	$\mathcal{D}R_1\varepsilon$	0.9554	4.9334
MV	$\mathrm{H}\mathcal{D}R_1\varepsilon$	0.8187	64.5810	$\mathrm{H}\mathcal{D}R_1\varepsilon$	0.8423	65.9762	$\mathrm{H}\mathcal{D}R_1\varepsilon$	0.8431	73.5649

4.1. Best fit fourth order regression models

In this subsection, we present the fourth order regression models for the eight physico-chemical properties. Based on the R^2 and $RMSE$ values we obtained the following best fit fourth order regression models for the physico-chemical properties.

$$BP = 2e-07(\mathcal{D}R_1\varepsilon)^4 - 0.0003(\mathcal{D}R_1\varepsilon)^3 + 0.1557(\mathcal{D}R_1\varepsilon)^2 - 30.235(\mathcal{D}R_1\varepsilon) + 2399.2 \tag{4.2}$$

$$E = 3e-08(\mathcal{D}R_1\varepsilon)^4 - 4E-05(\mathcal{D}R_1\varepsilon)^3 + 0.0211(\mathcal{D}R_1\varepsilon)^2 - 4.1382(\mathcal{D}R_1\varepsilon) + 342.92 \tag{4.3}$$

$$FP = -6e-13(H\mathcal{D}R_1\varepsilon)^4 + 9E-09(H\mathcal{D}R_1\varepsilon)^3 - 4E-05(H\mathcal{D}R_1\varepsilon)^2 + 0.0913(H\mathcal{D}R_1\varepsilon) + 186.46 \tag{4.4}$$

$$MR = -3e-08(\mathcal{D}R_1\varepsilon)^4 + 4E-05(\mathcal{D}R_1\varepsilon)^3 - 0.0212(\mathcal{D}R_1\varepsilon)^2 + 4.7925(\mathcal{D}R_1\varepsilon) - 284.37 \tag{4.5}$$

$$PSA = 1e-07(\mathcal{D}R_1\varepsilon)^4 - 0.0002(\mathcal{D}R_1\varepsilon)^3 + 0.1117(\mathcal{D}R_1\varepsilon)^2 - 22.298(\mathcal{D}R_1\varepsilon) + 1544.4 \tag{4.6}$$

$$P = -1e-08(\mathcal{D}R_1\varepsilon)^4 + 2E-05(\mathcal{D}R_1\varepsilon)^3 - 0.0084(\mathcal{D}R_1\varepsilon)^2 + 1.8909(\mathcal{D}R_1\varepsilon) - 112.02 \tag{4.7}$$

$$T = 2e-17(H\mathcal{D}R_2\varepsilon)^4 - 7E-12(H\mathcal{D}R_2\varepsilon)^3 + 5E-07(H\mathcal{D}R_2\varepsilon)^2 - 0.0099(H\mathcal{D}R_2\varepsilon) + 100.2 \tag{4.8}$$

$$MV = -2e-07(\mathcal{D}R_1\varepsilon)^4 + 0.0003(\mathcal{D}R_1\varepsilon)^3 - 0.1535(\mathcal{D}R_1\varepsilon)^2 + 32.073(\mathcal{D}R_1\varepsilon) - 2037.6 \tag{4.9}$$

Table 14. Best predictive fits from fourth order regression models.

Property	Equation No.	Best Predictors	R^2	$RMSE$
BP	(4.2)	$\mathcal{D}R_1\varepsilon$	0.9995	9.7565
E	(4.3)	$\mathcal{D}R_1\varepsilon$	0.9978	2.8616
FP	(4.4)	$H\mathcal{D}R_1\varepsilon$	0.9704	36.6018
MR	(4.5)	$\mathcal{D}R_1\varepsilon$	0.9776	10.1867
PSA	(4.6)	$\mathcal{D}R_1\varepsilon$	0.9583	23.9260
P	(4.7)	$\mathcal{D}R_1\varepsilon$	0.9777	4.0273
T	(4.8)	$H\mathcal{D}R_2\varepsilon$	0.9996	1.0035
MV	(4.9)	$\mathcal{D}R_1\varepsilon$	0.9634	41.0211

From Table 14, it is clear that the mentioned indices can be used to predict all the physico-chemical properties of the COVID-19 drugs. From our analysis of the proposed indices, we observe that

- $\mathcal{D}R_1\varepsilon$ index can be used to predict the Boiling Point (BP), Enthalpy of Vaporization (E), Molar Refraction (MR), Polar Surface Area (PSA), Polarizability (P) and Molar Volume (MV) with the corresponding R^2 values as 0.9995, 0.9978, 0.9776, 0.9583, 0.9777 and 0.9634, respectively.
- $H\mathcal{D}R_1\varepsilon$ index can be used to predict the Flash Point (FP) with the corresponding R^2 value as 0.9704.
- $H\mathcal{D}R_2\varepsilon$ index can be used to predict the Surface Tension (T) with the corresponding R^2 value as 0.9996.

Figure 6 to Figure 8 show the plots of the fourth order regression equations for Boiling Point (BP), Enthalpy of Vaporization (E), Molar Refraction (MR), Polar Surface Area (PSA), Polarizability (P) and Molar Volume (MV) with respect to $\mathcal{D}R_1\varepsilon$ index. Figure 9 shows the plots for Flash Point (FP) and Surface Tension (T) with respect to $H\mathcal{D}R_1\varepsilon$ and $H\mathcal{D}R_2\varepsilon$ indices, respectively.

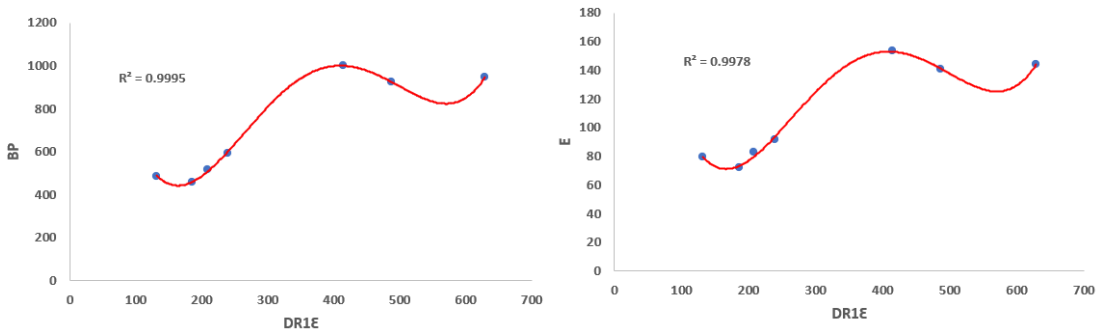

Figure 6. Fourth Order Regression Curves for BP and E against $\mathcal{D}R_1\varepsilon$.

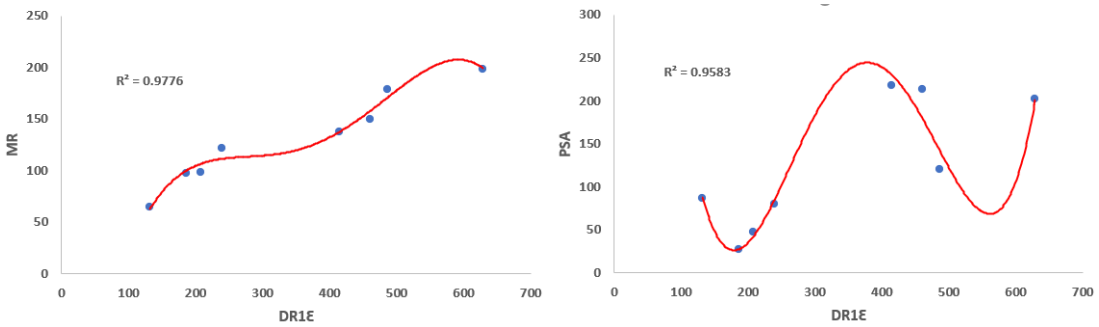

Figure 7. Fourth Order Regression Curves for MR and PSA against $\mathcal{D}R_1\varepsilon$.

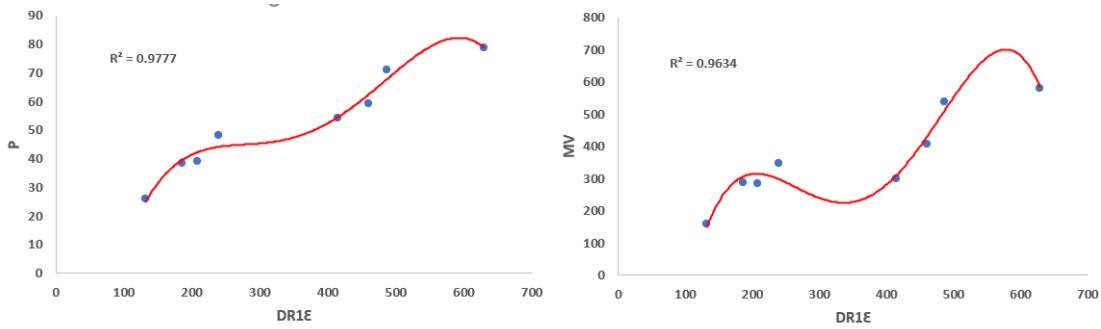

Figure 8. Fourth order regression curves for P and MV against $\mathcal{D}R_1\varepsilon$.

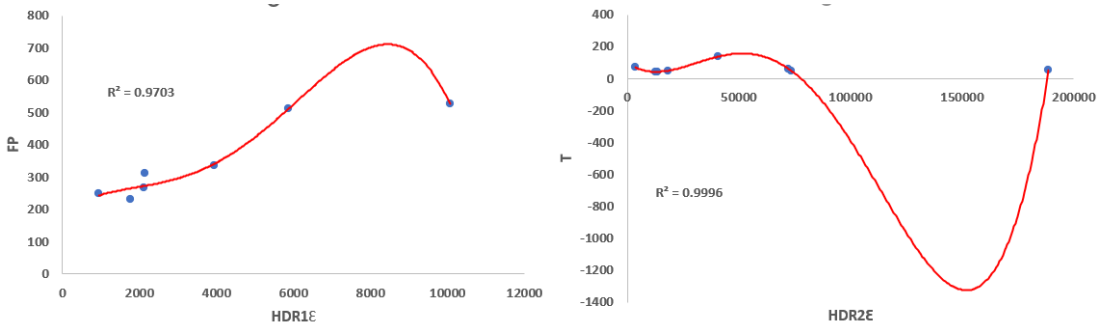

Figure 9. Fourth order regression curves for FP and T against $H\mathcal{D}R_1\varepsilon$ and $H\mathcal{D}R_2\varepsilon$, respectively.

4.2. Ediz eccentric connectivity index

In this section, we compare the predictive capability of our proposed indices against the ediz eccentric connectivity index. Table 15 shows the comparison of fourth order regression models of ediz eccentric connectivity index ($E\mathcal{E}^cI$) aganist the fourth order regression models based on our proposed indices.

Table 15. Comparison of predictive fits from $E\mathcal{E}^cI$ and proposed indices.

Property	Ediz	R^2	$RMSE$	Proposed Indices	R^2	$RMSE$
BP	$E\mathcal{E}^cI$	0.5516	280.5630	$\mathcal{D}R_1\varepsilon$	0.9995	9.7565
E	$E\mathcal{E}^cI$	0.5696	40.0779	$\mathcal{D}R_1\varepsilon$	0.9978	2.8616
FP	$E\mathcal{E}^cI$	0.3588	170.2130	$H\mathcal{D}R_1\varepsilon$	0.9704	36.6018
MR	$E\mathcal{E}^cI$	0.2212	60.0279	$\mathcal{D}R_1\varepsilon$	0.9776	10.1867
PSA	$E\mathcal{E}^cI$	0.8423	46.5065	$\mathcal{D}R_1\varepsilon$	0.9583	23.9260
P	$E\mathcal{E}^cI$	0.2227	23.7770	$\mathcal{D}R_1\varepsilon$	0.9777	4.0273
T	$E\mathcal{E}^cI$	0.9607	9.5006	$H\mathcal{D}R_2\varepsilon$	0.9996	1.0035
MV	$E\mathcal{E}^cI$	0.1849	193.6289	$\mathcal{D}R_1\varepsilon$	0.9634	41.0211

From Table 15, based on R^2 and $RMSE$ values it can be observed that the fourth order regression models based on our proposed indices provide the best fits for the eight physico-chemical properties.

5. Multilinear regression analysis of COVID-19 drugs

In this section we present the Multilinear regression analysis performed for the eight physico-chemical properties aganist our proposed indices. The general form of Multilinear regression is

$$P = \tilde{\alpha}_1(TI)_1 + +\tilde{\alpha}_2(TI)_2 + ... + +\tilde{\alpha}_n(TI)_n + \tilde{\gamma} \tag{5.1}$$

where P is the physico-chemical property (dependent variable), $\tilde{\gamma}$ is the regression model constant and $\tilde{\alpha}_i$ are the regression coefficients for the topological descriptors.

5.1. Best fit multilinear regression models

In this subsection we present the Multilinear regression models and the analysis for the eight physico-chemical properties.

$$BP = 0.0165(\mathcal{D}R_1\varepsilon) - 0.5221(\mathcal{D}R_2\varepsilon) - 0.0187(H\mathcal{D}R_1\varepsilon) + 5.3124(H\mathcal{D}R_2\varepsilon) + 213.299 \tag{5.2}$$

$$E = 0,0029(\mathcal{D}R_1\varepsilon) - 0.0869(\mathcal{D}R_2\varepsilon) - 0.0036(H\mathcal{D}R_1\varepsilon) + 0.8214(H\mathcal{D}R_2\varepsilon) + 41.6226 \tag{5.3}$$

$$FP = -0.0005(\mathcal{D}R_1\varepsilon) + 0.1072(\mathcal{D}R_2\varepsilon) - 0.0122(H\mathcal{D}R_1\varepsilon) - 0.5611(H\mathcal{D}R_2\varepsilon) + 196.499 \tag{5.4}$$

$$MR = -0.0050(\mathcal{D}R_1\varepsilon) + 0,0144(\mathcal{D}R_2\varepsilon) + 0.0087(H\mathcal{D}R_1\varepsilon) - 0.21(H\mathcal{D}R_2\varepsilon) + 11.05149 \tag{5.5}$$

$$PSA = 0.0095(\mathcal{D}R_1\varepsilon) - 0.2453(\mathcal{D}R_2\varepsilon) - 0.0133(H\mathcal{D}R_1\varepsilon) + 1.9034(H\mathcal{D}R_2\varepsilon) + 16.6273 \tag{5.6}$$

$$P = -0.0020(\mathcal{D}R_1\varepsilon) + 0.0412(\mathcal{D}R_2\varepsilon) + 0.0034(H\mathcal{D}R_1\varepsilon) - 0.0828(H\mathcal{D}R_2\varepsilon) + 4.4940 \tag{5.7}$$

$$T = 0.0080(\mathcal{D}R_1\varepsilon) - 0.2286(\mathcal{D}R_2\varepsilon) - 0.0089(H\mathcal{D}R_1\varepsilon) + 1.6116(H\mathcal{D}R_2\varepsilon) + 49.2483 \tag{5.8}$$

$$MV = -0.0213(\mathcal{D}R_1\varepsilon) + 0.5142(\mathcal{D}R_2\varepsilon 0.0213) + 0.0312(H\mathcal{D}R_1\varepsilon)^2 - 2.2024(H\mathcal{D}R_2\varepsilon) + 39.4661 \tag{5.9}$$

Table 16. Best predictive fits from multilinear regression model.

Property	Equation No.	R^2	$RMSE$
BP	(5.2)	0.9975	20.8648
E	(5.3)	0.9950	4.3123
FP	(5.4)	0.9495	47.7738
MR	(5.5)	0.9705	11.6830
PSA	(5.6)	0.7812	54.7782
P	(5.7)	0.9708	4.6056
T	(5.8)	0.8872	16.1008
MV	(5.9)	0.9137	63.0190

From Table 16, it can be observed that except for Polar Surface Area with $R^2 < 0.8$, all other properties are well predicted using the multilinear regression models.

5.2. QSAR analysis

The most generally used and useful indicator of a drug's effectiveness is its half-maximal inhibitory concentration IC_{50}. It is a quantitative metric that shows how much of a certain inhibitory substance (such as a medicine) is required in vitro to inhibit a specific biological process or biological component by 50 percent [33].

We fitted the Multilinear regression model given in Eq (5.10) to predict the IC_{50} values for the COVID-19 drugs.

$$IC_{50} = 0.0001(\mathcal{D}R_1\varepsilon) - 0.0081(\mathcal{D}R_2\varepsilon) + 0.0005(H\mathcal{D}R_1\varepsilon) + 0.0966(H\mathcal{D}R_2\varepsilon) - 4.2010 \tag{5.10}$$

The predicted IC_{50} values for the seven COVID-19 drugs, for which the experimental values are available, are presented in Table 17. It can be seen that the proposed multilinear regression model can be used to predict IC_{50} values.

Table 17. Experimental and calculated IC_{50} values of COVID-19 drugs.

Drug Name	$IC_{50}\ \mu M$	**Predicted IC_{50} using (5.10)**	**Absolute Residual**
Arbidol	3.54	3.342368	0.197632
Chloroquine	1.38	1.088041	0.291959
Hydroxy-Chloroquine	0.72	0.993671	0.27367
Lopinavir	5.25	3.880872	1.369128
Remdesivir	0.987	2.187685	1.20069
Ritonavir	8.63	8.627918	0.002082
Theaflavin	8.44	8.826445	0.38645

6. Conclusions

In this article, we proposed and computed the Diameter Eccentricity Based and Hyper Diameter Eccentricity Based topological descriptors for eight COVID-19 drugs, namely, Arbidol, Chloroquine, Hydroxy-Chloroquine, Lopinavir, Remdesivir, Ritonavir, Thalidomide and Theaflavin through $\mathcal{D}\varepsilon$-Polynomial. The indices were computed using our newly introduced $\mathcal{D}\varepsilon$- polynomial.

From the QSPR analysis using the curvilinear regression models, we conclude that the best fit fourth order regression models based on our proposed index $DR_1\varepsilon$ predict Boiling Point, Enthalpy of Vaporization, Molar Refraction, Polar Surface Area, Polarizability and Molar Volume. The fourth order regression models based on $DHR_1\varepsilon$ and $DHR_2\varepsilon$ can be used to predict Flash Point and Surface Tension, respectively.

We computed the Ediz Eccentric Connectivity index for COVID-19 drugs. Based on R^2 and $RMSE$ values, it can be observed that the fourth order regression models based on our proposed indices provide good predictions for the eight physico-chemical properties of the 8 COVID-19 drugs compared to the fourth order regression models based on the Ediz Eccentric Connectivity index.

Our proposed multilinear regression models provide good predictions for the physico-chemical properties expect the Polar Surface Area.

Multilinear regression model is best suited for predicting the 50% inhibitory concentration (IC_{50}) values with R^2 value 0.947.

The proposed indices can be used in designing new drugs to combat COVID-19 and other diseases.

Acknowledgement

The authors would like to thank the editor and reviewers for their helpful remarks in improving this manuscript. In addition, the authors would like to express their gratitude to the management of Vellore Institute of Technology, Chennai, India, for their encouragement and assistance in carrying out this research. This research work is financially supported by Vellore Institute of Technology, Chennai, India.

Use of AI tools declaration

The authors declare that they have not used artificial intelligence tools in the creation of this article.

Conflict of interest

The authors declare there is no conflict of interest.

References

1. M. Ahmad, D. Afzal, W. Nazeer, S. Kang, On topological indices of octagonal network, *Far East J. Math. Sci.*, **102** (2017), 2563–2571. https://dx.doi.org/10.17654/MS102112563
2. H. Wiener, Correlation of heats of isomerization, and differences in heats of vaporization of isomers, among the paraffin hydrocarbons, *J. Am. Chem. Soc*, **69** (1947), 2636–2638. https://doi.org/10.1021/ja01203a022
3. L. Feng, X. Zhu, W. Liu, Wiener index, Harary index and graph properties, *Discrete Appl. Math.*, **223** (2017), 72–83. https://doi.org/ 10.1016/j.dam.2017.01.028
4. G. Su, S. Wang, J. Du, M. Gao, K. Das, Y. Shang, Sufficient condition for a graph to be l-connected, l-Deficient, l-Hamiltonian and l^{-}-Independent in terms of the forgotten topological index, *Mathematics*, **10** (2022), 1802. https://doi.org/10.3390/math10111802
5. M. Ghorbani, A. H. Mohammad, A new version of Zagreb indices, *Filomat, JSTOR*, **26** (2012), 93–100. https://doi.org/10.2298/FIL1201093G
6. V. Sharma, R. Goswami, A. Madan, Eccentric connectivity index: A novel highly discriminating topological descriptor for structure- property and structure- activity studies, *J. Chem. Inf. Comput. Sci.*, **37** (1997), 273–282. https://doi.org/10.1021/ci960049h
7. I. Gutman, N. Trinajstic, Graph theory and molecular orbitals. Total π-electron energy of alternant hydrocarbons, *Chem. Phys. Lett.*, **17** (1972), 535–538. https://doi.org/ 10.1016/0009-2614(72)85099-1
8. S. Ghobadi, M. Ghorbaninejad, On F-polynomial, multiple and hyper F-index of some molecular graphs, *Bull. Math. Sci. Appl.*, **20** (2017), 36–43.
9. E. Estrada, L. Torres, L. Rodriguez, I. Gutman, An atom-bond connectivity index: Modelling the enthalpy of formation of alkanes, *Indian J. Chem.*, **37A** (1998), 849–855.
10. D. Vukicevic, B. Furtula, Topological index based on the ratios of geometrical and arithmetical means of end-vertex degrees of edges, *J. Math.*, **46** (2009), 1369–1376. https://doi.org/10.1007/s10910-009-9520-x
11. I. Gutman, Geometric approach to degree–based topological indices: Sombor indices, *Commun. Math. Comput. Chem.*, **86** (2021), 11–16.
12. Y. Shang, Sombor index and degree-related properties of simplicial networks, *Appl. Math. Comput.*, **419** (2022), 126881. https://doi.org/10.1016/j.amc.2021.126881
13. B. Bollobas, P. Erdos, Graphs of extremal weights, *Ars Combinatoria*, **50** (1998), 225–233. https://digitalcommons.memphis.edu/facpubs/4851
14. S. Fajtlowicz, On conjectures of graffiti, *Discrete Math.*, **72** (1988), 113–118. https://doi.org/10.1016/S0167-5060(08)70776-3

15. G. Li. E. de Clercq, Therapeutic options for the 2019 novel coronavirus (2019-nCoV), *Nat. Rev.*, **19** (2020), 149–150. https://doi.org/10.1038/d41573-020-00016-0

16. S. M. Hosamani, Quantitative structure property analysis of anti-Covid-19 drugs, preprint, arXiv: 2008.07350. https://doi.org/10.48550/arXiv.2008.07350

17. S. Gupta, M. Singh, A. K. Madan, Eccentric distance sum: A novel graph invariant for predicting biological and physical properties, *J. Math. Anal. Appl.*, **275** (2002), 386–401. https://doi.org/10.1016/S0022-247X(02)00373-6

18. H. Hua, K. Xu, W. Shu, A short and unified proof of Yu et al.'s two results on the eccentric distance sum, *J. Math. Anal. Appl.*, **382** (2011), 364–366. https://doi.org/10.1016/j.jmaa.2011.04.054

19. G. Yu, L. Feng, A. Ilic, On the eccentric distance sum of trees and unicyclic graphs, *J. Math. Anal. Appl.*, **375** (2010), 99–107. https://doi.org/10.1016/j.jmaa.2010.08.054

20. S. Mondal, N. De, A. Pal, Topological indices of some chemical structures applied for the treatment of COVID-19 Patients, *Polycyclic Aromat. Compd.*, (2020), 1220–1234. https://doi.org/10.1080/10406638.2020.1770306

21. V. Ravi, M. K. Siddiqui, N. Chidambaram, K. Desikan, On topological descriptors and curvilinear regression analysis of antiviral drugs used in COVID-19 treatment, *Polycyclic Aromat. Compd.*, (2021), 6932–6945. https://doi.org/10.1080/10406638.2021.1993941

22. S. A. K. Kirmani, P. Ali, F. Azam, Topological indices and QSPR/QSAR analysis of some antiviral drugs being investigated for the treatment of COVID-19 patients, *Int. J. Quantum Chem.*, **121** (2020), e26594. https://doi.org/10.1002/qua.26594

23. S. S. Shirkol, M. Kalyanshetti, S. M. Hosamani, QSPR analysis of certain distance based topological indices, *Appl. Math. Nonlinear Sci.*, **4** (2019), 371–386. https://doi.org/10.2478/AMNS.2019.2.00032

24. B. Lučić, I. Lukovits, S. Nikolić, N. Trinajstić, Distance-related indexes in the quantitative structure- property relationship modeling, *J. Chem. Inf. Comput. Sci.*, **41** (2001), 527–535. https://doi.org/10.1021/ci0000777

25. E. Deutsch, S. Klavžar, M-polynomial and degree-based topological indices, preprint, arXiv: 1407.1592v1. https://doi.org/10.48550/arXiv.1407.1592

26. S. Mondal, M. K. Siddiqui, N. De, A. Pal, Neighborhood M-polynomial of crystallographic structures, *Biointerface Res. Appl. Chem.*, **11** (2021), 9372–9381. https://doi.org/10.1155/2023/4668505

27. A. Saleh, G. B. Shalini, B. V. Dhananjayamurthy, The reduced neighborhood topological indices and RNM-polynomial for the treatment of COVID-19, *Biointerface Res. Appl. Chem.*, **11** (2021), 11817–11812. https://doi.org/10.33263/BRIAC114.1181711832

28. D. B. West, *Introduction to Graph Theory*, Prentice hall Upper Saddle River, **2** (2001).

29. D. Lee, M. K. Jamil, M. R. Farahani, H. M. Rehman, The ediz eccentric connectivity index of polycyclic aromatic hydrocarbons pahk, *Scholars J. Eng. Technol.*, **4** (2016), 148–152.

30. V. Kulli, Revan indices of oxide and honeycomb networks, *Int. J. Math. Appl.*, **55** (2017), 7.

31. V. Kulli, Hyper-Revan indices and their polynomials of silicate networks, *Int. J. Curr. Res. Sci. Technol.*, **4** (2018), 17–21.

32. A. Mahboob, G. Muhiuddin, I. Siddique, S. M. Alam, A view of Banhatti and Revan indices in chemical graphs, *J. Math.*, (2022), 5680712. https://doi.org/10.1155/2022/5680712

33. B. Chaluvaraju, A. B. Shaikh, Different versions of atom-bond connectivity indices of some molecular structures: Applied for the treatment and prevention of COVID-19, *Polycyclic Aromat. Compd.*, **42** (2022), 3748–3761. https://doi.org/10.1080/10406638.2021.1872655

AIMS Press